

# IF equation: a feature extractor for high-concentration time-frequency representation of mixed signals

Xiangxiang Zhu, Kunde Yang, Zhuosheng Zhang

**Abstract**—High-concentration time-frequency (TF) representation provides a valuable tool for characterizing multi-component non-stationary signals. In our previous work, we proposed using an instantaneous frequency (IF) equation to sharpen the TF distribution, and experiments verified its effectiveness. In this paper, we systematically discuss why the IF equation-based TF analysis methods work and how to use the IF equation to improve TF sharpness. By the analysis of the properties of the IF equation, we prove that a good IF equation can unify the well-known IF and group delay estimators and provides an effective way to characterize the mixture of time-varying and frequency-varying signals. By discussing the post-processing techniques based on the IF equation, we can prove that many popular TF post-processing methods, such as the synchroextracting transform, the multi-synchrosqueezing transform, and the time extracting transform, fall into the IF equation-based category. We also propose a novel approach to combine different IF equations to minimize energy spreading based on local sparsity. Numerical simulations and practical experiments are presented to illustrate the performance of the proposed IF equation-based TF analysis method.

**Index Terms**—High-resolution time-frequency analysis, Synchrosqueezing transform, Synchroextracting transform, IF equation, Mixed signals.

## I. INTRODUCTION

**T**he study and the interpretation of multi-component non-stationary signals require a powerful analysis tool. Time-frequency (TF) analysis methods are used to measure how a signal's frequency components vary with time and provide an effective tool in non-stationary signals analysis [1-7]. The most frequently used TF representation is the linear TF analysis method, mainly including the short-time Fourier transform (STFT) [8], the continuous wavelet transform (CWT) [9], the Stockwell transform [10], and the chirplet transform (CT) [11]. This kind of method characterizes the signal via inner products with a pre-assigned basis and has invertibility and low computation cost. However, restricted by the Heisenberg uncertainty principle [12], the linear TF analysis can not

simultaneously obtain optimal time and frequency resolution, easily leading to a blurred TF representation.

To solve the above limitation, the post-processing methods of the linear TF representations have been widely studied in the past decades. The reassignment method (RM), proposed by Koderer et al. to the spectrogram [13] and generalized by F. Auger and P. Flandrin to the time-scale distribution and others [14], reassigns the TF energy from the original position to the gravity center of the signal's energy distribution such that a sharpened TF representation is yielded. F. Auger et al. also extended the standard RM to the Levenberg-Marquardt reassignment [15], making the concentration of the signal energy adjustable. J. Xiao and P. Flandrin [16] presented the multitaper TF reassignment with the two-fold objective of a sharp localization for the chirp components and a reduced level of statistical fluctuations for the noise. In [17], Bruni et al. proposed a modified RM for analyzing multi-component crossing signals with cross-over instantaneous frequencies (IFs). This method corrects the TF result of the standard RM in the non-separable region partly. In [18], a multitaper reassigned spectrogram was proposed for oscillating transients with Gaussian envelopes, which localizes energy at the instantaneous frequency (IF) of transients, while Gaussian white noise is made flatter by the use of multiple windows. In [19], an iterative reassignment method was presented to extract transient features of strongly time-varying signals and frequency-varying signals. Although RM and its variants improve the energy concentration of the linear TF representation, they lack an explicit formula for signal reconstruction, which limits its application [20].

Another popular TF post-processing method is the synchrosqueezing transform (SST), initialized in [21] and further analyzed in [22]. This method was developed in understanding the principle of the empirical mode decomposition [23]. By squeezing the TF coefficients into the IF trajectory in the frequency direction, SST not only enhances TF readability but also allows for mode retrieval. Because of the advantages of mode representation and reconstruction, many new developments of SST have been carried out in various directions. First, an extension to the STFT case was proposed in [24], while a generalization of the wavelet approach utilizing wavelet packet decomposition for both one-dimensional and two-dimensional cases was available in [25,26]. Extensions to other transform frameworks included, but not limited to, the synchrosqueezing S-transform [27], the synchrosqueezing three-parameter wavelet transform [28], and the fractional synchrosqueezing

This work was supported by the Natural Science Foundation of Shaanxi Province under Grant 2023-JC-QN-0739, the Guangdong Basic and Applied Basic Research Foundation under Grant no. 208058579085, the National Natural Science Foundation of China under Grant no. U20B2075, the Fundamental Research Funds for the Central Universities under Grant no. G2021KY05103.

X. Zhu is with School of Mathematics and Statistics, Northwestern Polytechnical University, Xi'an 710072, China (e-mail: zhuxiangxiang@nwpu.edu.cn)

K. Yang is with School of Marine Science and Technology, Northwestern Polytechnical University, Xi'an 710072, China (e-mail: ykdzym@nwpu.edu.cn).

Z. Zhang is with School of Mathematics and Statistics, Xi'an Jiaotong University, Xi'an, 710049, China (e-mail: zszhang@mail.xjtu.edu.cn).

transformation [29]. Second, the robust analysis of SST has been studied in [30-32] and a new IF estimator within the framework of the signal's phase derivative and the linear canonical transform was introduced in [33]. Moreover, a study of SST applied to multivariate data was done in [34]. An adaptive SST with a time-varying parameter was introduced in [35,36], which obtains the well-separated condition for multi-component signals using the linear frequency modulation to approximate a non-stationary signal at every time instant. The theoretical analysis of adaptive SST was studied in [37,38]. Finally, combining the SST with the ideal TF representation theory, the synchroextracting transform (SET) [39] was proposed to improve the TF concentration by extracting the ridges of the STFT.

SST works well for sinusoidal signals but suffers from low TF resolution when dealing with strong modulation signals that consist of a fast-varying feature. To address this drawback, many improvements have been presented, mainly including the demodulated SST [40,41], the high-order SST [42,43], the multi-synchrosqueezing transform [44,45], and the time-reassigned SST [46,47]. The demodulated SSTs [40,41] aim to change broad-band signals to narrow-band signals and the standard SST is followed then. The high-order SSTs [42,43] aim to calculate an IF estimation in the TF or time-scale domain for more general signal types. The multi-synchrosqueezing transformations [44,45] apply an iterative reassignment technique to sharpen the blurred TF energy step-by-step. The time-reassigned SSTs [46,47], in fact, introduce a dual operator by considering time reassignment instead of frequency reassignment and have a good performance in addressing pulsed-like signals. A comprehensive review of the subject of reassigned TF representations is provided in Ref. [5,20].

The mechanism of the SST and its variants introduced above is to derive an IF or group delay (GD) estimator for different transform frameworks and different-type signals, and further to reassign TF coefficients from the original position to the estimated instantaneous trajectories. Indeed, the IF (or GD) estimator is critical to this kind of method (we can denote it as the IF estimator-based TF post-processing method) because it determines the accuracy of high-concentration TF representations. Instead of computing the IF (or GD) estimation, another high-concentration TF representation is based on the IF equation [48-50], i.e., a non-linear function in the TF domain with the IFs of the signal as its solution. This kind of method (denoted as the IF equation-based TF post-processing method) enhances the TF concentration by solving the IF equation using the fixed point iterative algorithm [48] or the extractor [49,50] and has been used in the sound signal analysis [48,49], mechanical signal processing [51], and medical data analysis [52]. Several issues about the IF equation-based TF post-processing methods, however, should be considered. First, theoretical analysis of the IF equation and how to use it to concentrate the TF distribution should be explained more comprehensively, involving the definition and properties of the IF equation, and the convergence of its solution algorithm. Second, we know an IF estimator or GD estimator can not simultaneously characterize the time-varying

and frequency-varying information of a mixed signal. How about the IF equation? Last but not least, we should consider if there is a theoretical model to cover the prevailing TF analysis methods, including the SET [39], the multi-synchrosqueezing transformation [44], and the time synchroextracting transform [52].

In this paper, we focus on the IF equation-based TF post-processing methods and attempt to build a theoretical framework for it. We first review the IF estimator-based TF post-processing methods and then define the IF equation followed by three concrete expressions under the STFT framework. We study the properties of the IF equation, and introduce two ways, that is, by the extractor to detect signal information and by iterative algorithms for TF reassignment, to concentrate the TF localization using the IF equation. The difference between the IF estimator-based methods and the IF equation-based methods is discussed. By analysis, a significant advantage of the IF equation-based methods over the former is that a good IF equation contains not only the IF information but also the GD information, which can unify the IF and GD estimators and characterizes mixed signals effectively. By combining two IF equations, a novel TF analysis approach is proposed to further minimize energy spread based on local sparsity. Finally, numerical examples of the theoretical derivations are presented. The potential applications are also explored and verified.

The remainder of the paper is organized as follows. In Section II, we review the IF estimator-based TF post-processing methods. Section III presents the proposed IF equation-based TF post-processing methods with definition, properties, and post-processing technologies. Section IV proposes a combination of extracting transform with different IF equations. Comparative studies and applications are presented in Section V. Finally, the conclusions are drawn in Section VI.

## II. A REVIEW OF THE IF ESTIMATOR-BASED TF POST-PROCESSING METHODS

### A. Signal model

Multi-component non-stationary signals are comprised of several mono-components and form the general case. In this paper we use the popular amplitude-modulation and frequency-modulation (AM-FM) model to describe the time-varying features of multi-component non-stationary signals, which is defined as

$$f(t) = \sum_{k=1}^K f_k(t) = \sum_{k=1}^K A_k(t) e^{j\phi_k(t)}, \quad (1)$$

where  $K$  is a positive integer representing the number of AM-FM components,  $j$  denotes the imaginary unit with  $j^2 = -1$ ,  $A_k(t) > 0$  and  $\phi_k(t)$  denote the instantaneous amplitude and instantaneous phase of the  $k$ -th component (or mode), respectively. The first and the second derivatives of the phase, i.e.,  $\phi'_k(t)$ ,  $\phi''_k(t)$ , are referred to as the instantaneous frequency (IF) and chirp rate (CR) of the  $k$ -th component.

### B. IF estimator-based TF post-processing method

The TF post-processing methods, originating from the RM [14] and SST [22], relocate the original TF points to concentrate the spread TF distribution. With this regard, a crucial problem is to determine where the blurred TF points are rearranged. The ideal one, of course, is moved to the true IF curves of the signal analyzed, which thus drives the study of the IF estimators in the TF domain. Under the STFT framework, we give an introduction to the IF estimator-based TF post-processing methods.

Given signal  $f(t) \in L^2(\mathbb{R})$ , its Fourier transform is defined as

$$\hat{f}(\omega) = \int_{-\infty}^{+\infty} f(t)e^{-j\omega t} dt. \quad (2)$$

The (modified) STFT of  $f(t)$ , which is obtained through the use of a sliding window  $g(t) \in L^2(\mathbb{R})$ , is given by

$$S_f^g(t, \omega) = \int_{-\infty}^{+\infty} f(\mu)g^*(\mu - t)e^{-j\omega(\mu - t)} d\mu, \quad (3)$$

where the superscript  $*$  denotes the complex conjugate. It is known that the STFT can not simultaneously localize a signal in both time and frequency precisely due to the limitation of the Heisenberg uncertainty principle [12], i.e., a long window favors better concentration in frequency but worse temporal localization, while a short window provides good temporal localization but poor frequency resolution. To improve the TF localization precision and show good TF readability, the TF post-processing methods [22, 24, 25, 27, 42, 43] are presented to relocate the TF coefficients into the IF trajectories. Thanks to G. Thakur and H.T. Wu, they develop I. Daubechies's work [22] and give a two-dimensional IF estimator by STFT as follows [24]:

$$\hat{\omega}_1(t, \omega) = \Re \left\{ \frac{\frac{\partial}{\partial t} S_f^g(t, \omega)}{j S_f^g(t, \omega)} \right\}, \quad (4)$$

here  $|S_f^g(t, \omega)| > \lambda$  ( $\lambda > 0$ ), and  $\Re\{\cdot\}$  is the real part of complex number. The IF estimator (4) is accurate for the harmonic-like signals with the stationary instantaneous feature, i.e., each model of the signal  $f(t)$  satisfies  $|A'_k(t)| < \epsilon$ ,  $|\phi''_k(t)| < \epsilon$  for  $k = 1, 2, \dots, K$  (here  $\epsilon$  is a small positive constant).

With the IF estimator  $\hat{\omega}_1(t, \omega)$  defined by (4), the STFT-based SST (FSST) [24] is to reassign the TF coefficients from the original location to the estimated IF trajectory along the frequency direction:

$$T_f^1(t, \omega) = \int_{|S_f^g(t, \eta)| > \lambda} S_f^g(t, \eta) \delta(\omega - \hat{\omega}_1(t, \eta)) d\eta, \quad (5)$$

where  $\delta(\cdot)$  is the Dirac delta function.

FSST suffers from a low TF resolution at the modulated part of fast-varying signals, such as chirp-like signals. To address this shortcoming, paper [42] introduced another IF estimator as (6), where  $\tilde{q}(t, \omega)$  is given by

$$\tilde{q}(t, \omega) = \frac{\frac{\partial}{\partial t} \left( \frac{\frac{\partial}{\partial t} S_f^g(t, \omega)}{S_f^g(t, \omega)} \right)}{j - \frac{\partial}{\partial t} \left( \frac{\frac{\partial}{\partial \omega} S_f^g(t, \omega)}{S_f^g(t, \omega)} \right)}. \quad (7)$$

The quantity  $\hat{\omega}_2(t, \omega)$  corresponds to the true IFs of the Gaussian modulated linear chirp [42]. The second-order SST then consists in replacing  $\hat{\omega}_1(t, \omega)$  by  $\hat{\omega}_2(t, \omega)$  in the standard FSST:

$$T_f^2(t, \omega) = \int_{|S_f^g(t, \eta)| > \lambda} S_f^g(t, \eta) \delta(\omega - \hat{\omega}_2(t, \eta)) d\eta. \quad (8)$$

In fact, the IF estimator-based TF post-processing methods can be unified as

$$T_f(t, \omega) = \int_{|S(t, \eta)| > \lambda} S(t, \eta) \delta(\omega - \hat{\omega}(t, \eta)) d\eta, \quad (9)$$

where  $S(t, \eta)$  denotes a TF transform, and  $\hat{\omega}(t, \eta)$  is an IF estimator calculated in the TF domain. If the GD estimation  $\hat{t}(\mu, \omega)$  under the TF representation is known, the reassignment of the TF coefficients along the time direction can be similarly performed:

$$\tilde{T}_f(t, \omega) = \int_{|S(\mu, \omega)| > \lambda} S(\mu, \omega) \delta(t - \hat{t}(\mu, \omega)) d\mu. \quad (10)$$

The IF estimator-based TF methods are all that an IF (or GD) estimator is determined first in the transform domain and then a relocation step is performed. Different from the mechanism of this kind of method, in the following, we will introduce another class method, i.e., the IF equation-based TF post-processing method. This method can provide a high-concentration TF representation for the mixed signals.

### III. IF EQUATION-BASED TF POST-PROCESSING METHOD

The central idea of the IF equation-based TF post-processing method is to find an IF equation in the TF domain to characterize the instantaneous features of the signal. By solving the IF equation, it is expected to output a concentrated and accurate TF representation.

#### A. Definition of IF equation

**Definition 1.** For a multi-component non-stationary signal  $f(t) = \sum_{k=1}^K A_k(t)e^{j\phi_k(t)}$ , let  $\Omega$  be a set that  $\Omega \subset \{(t, \omega) | t \in \mathbb{R}, \omega > 0\}$  and  $(t, \phi'_k(t)) \in \Omega$ ,  $t \in \mathbb{R}$ ,  $k = 1, 2, \dots, K$ . A binary equation  $h_f(t, \omega) = 0$  is called the IF equation of  $f(t)$  on  $\Omega$  if, for any  $(t, \omega) \in \Omega$ , it satisfies

$$\begin{aligned} h_f(t, \omega) &= 0 \text{ if } \omega = \phi'_k(t) \text{ for an integer } k \in \{1, 2, \dots, K\}, \\ h_f(t, \omega) &\neq 0 \text{ if } \omega \neq \phi'_k(t) \text{ for any integer } k \in \{1, 2, \dots, K\}. \end{aligned} \quad (11)$$

From Definition 1, we know that the IF curves  $\omega = \phi'_k(t)$  of each model of  $f(t)$  are the solutions of its IF equation. Therefore, the IF equation, including the main information of the studied signal, can be considered a feature extractor.

In order to show the IF equation more clearly, we now consider a specific example of constant amplitude and linear frequency modulation signal (also known as chirp), i.e.,  $f(t) = Ae^{j\phi(t)}$ , where  $A$  is a positive constant,  $\phi(t) = a + bt + \frac{c}{2}t^2$ ,

$$\hat{\omega}_2(t, \omega) = \begin{cases} \Re \left\{ \frac{\frac{\partial}{\partial t} S_f^g(t, \omega)}{S_f^g(t, \omega)} \right\} + \Re \left\{ \tilde{q}(t, \omega) \frac{\frac{\partial}{\partial \omega} S_f^g(t, \omega)}{S_f^g(t, \omega)} \right\}, & \text{if } \frac{\partial}{\partial t} \left( \frac{\frac{\partial}{\partial \omega} S_f^g(t, \omega)}{S_f^g(t, \omega)} \right) \neq j, \text{ and } S_f^g(t, \omega) \neq 0, \\ \hat{\omega}_1(t, \omega), & \text{if } \frac{\partial}{\partial t} \left( \frac{\frac{\partial}{\partial \omega} S_f^g(t, \omega)}{S_f^g(t, \omega)} \right) = j, \text{ and } S_f^g(t, \omega) \neq 0, \end{cases} \quad (6)$$

$a, b, c$  are real numbers. In this case, the STFT under the Gaussian window  $g(t) = \frac{1}{\sqrt{2\pi}\sigma} e^{-\frac{t^2}{2\sigma^2}}$  is calculated as

$$\begin{aligned} S_f^g(t, \omega) &= \int_{-\infty}^{+\infty} f(\mu) g^*(\mu - t) e^{-j\omega(\mu - t)} d\mu \\ &= f(t) \frac{1}{\sqrt{1 - j\sigma^2 c}} \exp \left( -\frac{\sigma^2}{2} \frac{(\omega - \phi'(t))^2}{1 - j\sigma^2 c} \right), \end{aligned} \quad (12)$$

where  $\phi'(t) = b + ct$ . From (12), we can obtain that

$$\frac{\partial}{\partial \omega} S_f^g(t, \omega) = S_f^g(t, \omega) \left( -\frac{\sigma^2(\omega - \phi'(t))}{1 - j\sigma^2 c} \right). \quad (13)$$

The set of points  $\omega = \phi'(t)$  satisfies  $\left| \frac{\frac{\partial}{\partial \omega} S_f^g(t, \omega)}{S_f^g(t, \omega)} \right|^2 = 0$  for  $|S_f^g(t, \omega)| > \lambda$  (here  $0 < \lambda < \frac{A}{2\sqrt{1+\sigma^4 c^2}}$ ). Therefore, we can define an IF equation of  $f(t) = Ae^{j\phi(t)}$  on  $\Omega = \{(t, \omega) | t \in \mathbb{R}, \omega > 0, |S_f^g(t, \omega)| > \lambda\}$  as

$$IF_1 : \left| \frac{\frac{\partial}{\partial \omega} S_f^g(t, \omega)}{S_f^g(t, \omega)} \right|^2 = 0. \quad (14)$$

From (13), it is easy to see that the other two IF equations of the chirp signal  $f(t)$  on  $\Omega$  are formulated as

$$IF_2 : \Re \left\{ \frac{\frac{\partial}{\partial \omega} S_f^g(t, \omega)}{S_f^g(t, \omega)} \right\} = 0, \quad (15)$$

$$IF_3 : \Im \left\{ \frac{\frac{\partial}{\partial \omega} S_f^g(t, \omega)}{S_f^g(t, \omega)} \right\} = 0, \quad (16)$$

where  $\Im\{\cdot\}$  is the imaginary part of complex number. Therefore, the IF equation of the same signal is not unique. Various IF equations have different properties. By the numerical experiments (see Fig. 1), we will see that  $IF_2$  is more appropriate to characterize the time-varying signals, whereas  $IF_3$  is more effective when handling the frequency-varying signals. Thus, finding a powerful IF equation that covers as many signal types as possible and has some good properties for its solutions is an important work that needs attention and exploration.

The three equations can be more efficiently computed by

$$\frac{\partial}{\partial \omega} S_f^g(t, \omega) = S_f^{tg}(t, \omega) \quad \text{for } (t, \omega) \in \Omega, \quad (17)$$

where  $S_f^{tg}(t, \omega)$  denotes the STFT of  $f(t)$  using  $tg(t)$  as its window. It is also noted that other TF transformations or window functions can be used to define the IF equation. Indeed, we can define the IF equation of chirp signal similar to  $IF_1$ , ( $IF_2$  or  $IF_3$ ) if an even window function is employed.

In the following section, using  $IF_1$  as the main research object, we discuss some properties of the IF equation.

## B. Properties of the IF equation

1) *Existence and uniqueness*: The definition of the IF equation indicates that, for each time  $t$ ,  $\omega = \phi'(t)$  is the solution of  $IF_1$  over the set  $\Omega$ . If considering a mono-component chirp,  $\omega = \phi'(t)$  is the unique solution for each time  $t$ . This property is essential for detecting the signal feature because that can characterize the instantaneous information of the signal and exclude other unwanted information.

2) *Impulse signals detection*: The instantaneous information  $t = t_0$  of impulse signal  $f(t) = A\delta(t - t_0)$  is the unique solution of  $IF_1$  for the fixed  $\omega$ .

The STFT of the transient signal  $f(t) = A\delta(t - t_0)$  with the Gaussian window is computed as

$$S_f^g(t, \omega) = A(\sqrt{2\pi}\sigma)^{-1} e^{-\frac{(t-t_0)^2}{2\sigma^2}} e^{-j\omega(t-t_0)}. \quad (18)$$

From (18), we can obtain that

$$\left| \frac{\frac{\partial}{\partial \omega} S_f^g(t, \omega)}{S_f^g(t, \omega)} \right|^2 = (t - t_0)^2. \quad (19)$$

Therefore, for any  $\omega$ ,  $t = t_0$  is the unique solution of  $IF_1$ .

The  $IF_3$  also can characterize this impulse signal, whereas  $IF_2$  does not include the transient feature of the signal. Consequently, the  $IF_1$  and  $IF_3$  are more preferred than  $IF_2$  when dealing with impulse signals.

3) *Detection of transient signal with Gaussian envelope*: The TF centre  $(t_0, \omega_0)$  of an oscillating transient with a Gaussian envelope  $f(t) = Ae^{-\frac{(t-t_0)^2}{2\sigma_0^2}} e^{j\omega_0 t}$  is the unique solution of  $IF_1$ .

The STFT of signal  $f(t) = Ae^{-\frac{(t-t_0)^2}{2\sigma_0^2}} e^{j\omega_0 t}$  is computed as

$$\begin{aligned} S_f^g(t, \omega) &= (\sqrt{2\pi}\sigma)^{-1} f(t) \int_{-\infty}^{+\infty} e^{-\frac{(t-t_0)\mu}{\sigma_0^2}} e^{-\frac{\mu^2}{2}(\frac{1}{\sigma_0^2} + \frac{1}{\sigma^2})} e^{-j(\omega - \omega_0)\mu} d\mu, \\ &= f(t) e^{\frac{\sigma^2}{2\sigma_0^2(\sigma^2 + \sigma_0^2)}(t-t_0)^2} e^{-\frac{\sigma^2\sigma_0^2}{2(\sigma^2 + \sigma_0^2)}(\omega - \omega_0)^2} e^{j\frac{\sigma^2}{\sigma^2 + \sigma_0^2}(t-t_0)(\omega - \omega_0)}. \end{aligned} \quad (20)$$

From (20), it follows that

$$\left| \frac{\frac{\partial}{\partial \omega} S_f^g(t, \omega)}{S_f^g(t, \omega)} \right|^2 = \left| -\frac{\sigma^2\sigma_0^2}{\sigma^2 + \sigma_0^2}(\omega - \omega_0) + j\frac{\sigma^2}{\sigma^2 + \sigma_0^2}(t - t_0) \right|^2, \quad (21)$$

Thus the point  $(t_0, \omega_0)$  is the unique solution of  $IF_1$  to make

$$h_f(t, \omega) := \left| \frac{\frac{\partial}{\partial \omega} S_f^g(t, \omega)}{S_f^g(t, \omega)} \right|^2 = 0.$$

4) *Linear group delay detection*: For any  $\omega$ , the GD of linear group delay signal  $\hat{f}(\omega) = Ae^{-j(a+b\omega+\frac{c}{2}\omega^2)}$  is the unique solution of  $IF_1$ .

Since the STFT of  $f(t)$  can be rewritten as

$$\begin{aligned} S_f^g(t, \omega) &= \int_{-\infty}^{+\infty} f(\mu)g^*(\mu - t)e^{-j\omega(\mu - t)}d\mu \\ &= \frac{1}{2\pi} \int_{-\infty}^{+\infty} \hat{f}(\nu)\hat{g}^*(\nu - \omega)e^{jt\nu}d\nu, \end{aligned} \quad (22)$$

then the STFT of linear group delay model can be expressed as

$$S_f^g(t, \omega) = \frac{1}{2\pi} \hat{f}(\omega)e^{jt\omega} \int_{-\infty}^{+\infty} e^{-j\frac{\sigma}{2}\nu^2} \hat{g}^*(\nu)e^{j(t-b-c\omega)\nu}d\nu. \quad (23)$$

From (23), we have

$$\begin{aligned} \frac{\partial}{\partial \omega} S_f^g(t, \omega) &= j(t - b - c\omega) S_f^g(t, \omega) \\ &- \frac{j\sigma}{2\pi} \hat{f}(\omega)e^{jt\omega} \int_{-\infty}^{+\infty} e^{-j\frac{\sigma}{2}\nu^2} \nu \hat{g}^*(\nu)e^{j(t-b-c\omega)\nu}d\nu. \end{aligned} \quad (24)$$

Due to the Fourier transform of Gaussian window  $g(t) = \frac{1}{\sqrt{2\pi}\sigma} e^{-\frac{t^2}{2\sigma^2}}$  is calculated as

$$\hat{g}(\nu) = e^{-\frac{\sigma^2}{2}\nu^2}, \quad (25)$$

which yields that

$$\int_{-\infty}^{+\infty} e^{-j\frac{\sigma}{2}\nu^2} \nu \hat{g}^*(\nu)d\nu = 0.$$

Consequently,  $t = b + c\omega$  satisfies  $h_f(b + c\omega, \omega) = 0$ . The uniqueness of the solution can be proved by deducing the expression of (23) using (25) for the linear group delay signal (one can refer to the calculation of (12)).

This result shows a clear advantage of the IF equation over the IF estimator since  $IF_1$  covers the instantaneous characteristic of both the chirp signal and the linear group delay model, unifying the well-known IF and GD estimators proposed in the SST [22,24] and the time-reassigned SST [46].

5) *Characterizing a mixture of harmonic-like and pulsive-like signals*: Let  $f(t) = A_1 e^{j\omega_1 t} + A_2 e^{-\frac{(t-t_2)^2}{2\sigma^2}} e^{j\omega_2 t}$  be a multi-component signal consisting of harmonic and pulse components. Suppose the support of  $e^{-\frac{\sigma^2}{2}\omega^2}$  be  $[-\Delta, \Delta]$ , and the parameter of  $\sigma$  of the Gaussian window used in the STFT be taken as  $\sigma = l\tilde{\sigma}$ , here  $l > 0$ . If  $|\omega_1 - \omega_2| > \frac{\sqrt{1+l^2}}{l}\Delta$ , then

$$h_f(t, \omega_1) = 0 \text{ and } h_f(t_2, \omega_2) = 0.$$

The STFT of the two-component signal  $f(t)$  under the Gaussian window is that

$$\begin{aligned} S_f^g(t, \omega) &= f_1(t)e^{-\frac{l^2\tilde{\sigma}^2}{2}(\omega-\omega_1)^2} + \frac{A_2}{\sqrt{1+l^2}} e^{-\frac{l^2\tilde{\sigma}^2}{2(1+l^2)}(\omega-\omega_2)^2} \times \\ &e^{-\frac{(t-t_2)^2}{2(1+l^2)\tilde{\sigma}^2}} e^{j\frac{l^2}{1+l^2}(\omega-\omega_2)(t-t_2)} e^{j\omega_2 t}. \end{aligned} \quad (26)$$

Thus, we have

$$\begin{aligned} \frac{\partial}{\partial \omega} S_f^g(t, \omega) &= -l^2\tilde{\sigma}^2 f_1(t)(\omega - \omega_1)e^{-\frac{l^2\tilde{\sigma}^2}{2}(\omega-\omega_1)^2} \\ &- \frac{A_2 l^2 \tilde{\sigma}^2}{\sqrt{1+l^2}(1+l^2)} (\omega - \omega_2)e^{-\frac{l^2\tilde{\sigma}^2}{2(1+l^2)}(\omega-\omega_2)^2} e^{-\frac{(t-t_2)^2}{2(1+l^2)\tilde{\sigma}^2}} \times \\ &e^{j\frac{l^2}{1+l^2}(\omega-\omega_2)(t-t_2)} e^{j\omega_2 t} + \frac{jA_2 l^2}{\sqrt{1+l^2}(1+l^2)} e^{-\frac{l^2\tilde{\sigma}^2}{2(1+l^2)}(\omega-\omega_2)^2} \times \\ &(t - t_2)e^{-\frac{(t-t_2)^2}{2(1+l^2)\tilde{\sigma}^2}} e^{j\frac{l^2}{1+l^2}(\omega-\omega_2)(t-t_2)} e^{j\omega_2 t}. \end{aligned} \quad (27)$$

Due to

$$\begin{aligned} \left| \frac{\partial}{\partial \omega} S_f^g(t, \omega_1) \right| &\leq \frac{A_2 l^2 \tilde{\sigma}^2}{(1+l^2)^{\frac{3}{2}}} |\omega_1 - \omega_2| e^{-\frac{l^2\tilde{\sigma}^2}{2(1+l^2)}(\omega_1-\omega_2)^2} \\ &+ \frac{A_2 l^2}{(1+l^2)^{\frac{3}{2}}} e^{-\frac{l^2\tilde{\sigma}^2}{2(1+l^2)}(\omega_1-\omega_2)^2} |t - t_2| e^{-\frac{(t-t_2)^2}{2(1+l^2)\tilde{\sigma}^2}} \\ &\leq C e^{-\frac{l^2\tilde{\sigma}^2}{2(1+l^2)}(\omega_1-\omega_2)^2}, \end{aligned}$$

where  $C = \frac{A_2 l^2 \tilde{\sigma}^2}{(1+l^2)^{\frac{3}{2}}} |\omega_1 - \omega_2| + \frac{A_2 l^2 \tilde{\sigma}}{e^{\frac{1}{2}(1+l^2)}}$ . The fact that  $|\omega_1 - \omega_2| > \frac{\sqrt{1+l^2}}{l}\Delta$  and the support of  $e^{-\frac{\sigma^2}{2}\omega^2}$  is  $[-\Delta, \Delta]$  leads to  $\left| \frac{\partial}{\partial \omega} S_f^g(t, \omega_1) \right| = 0$ , therefore we have  $h_f(t, \omega_1) = 0$ . Similarly, it can be obtained that

$$\left| \frac{\partial}{\partial \omega} S_f^g(t_2, \omega_2) \right| = l^2 \tilde{\sigma}^2 A_1 |\omega_2 - \omega_1| e^{-\frac{l^2\tilde{\sigma}^2}{2}(\omega_2-\omega_1)^2},$$

which also yields  $h_f(t_2, \omega_2) = 0$ . Therefore,  $IF_1$  extracts the instantaneous information of signals consisting of a mixture of harmonic-like and pulsive-like components.

6) *Combination of IF equations*: It is known that a single window is difficult to balance time resolution and frequency resolution. The combination of multiple spectrograms or wavelet transforms with short and long windows or a set of wavelets has been shown to result in good joint TF resolution for signals consisting of mixtures of tones and pulses [50,54]. Inspired by this idea, we can also define a multi-resolution IF equation of chirp (impulse or linear group delay) signal:

$$MrIF(t, \omega) := \left| \left( \prod_{i=1}^m \frac{\frac{\partial}{\partial \omega} S_f^{g_i}(t, \omega)}{S_f^{g_i}(t, \omega)} \right)^{\frac{1}{m}} \right| = 0, \quad (28)$$

for  $|S_f^{g_i}(t, \omega)| > \lambda$ . Here  $S_f^{g_i}(t, \omega)$  denotes the STFT of  $f(t)$  using the Gaussian window with parameter  $\sigma_i$ . This equation corresponds to the geometric mean of multiple IF equations and is built on high-resolution TF representation. In this regard, it can be used to characterize the signal with closely-spaced instantaneous information [50]. It should be pointed out that, except for geometric mean, one can explore other combination forms of IF equations for non-stationary signals analysis.

### C. TF post-processing method using IF equation

This section introduces how to use the given IF equation  $h_f(t, \omega) = 0$  to concentrate the spread TF distribution. Generally, there are two classical ways to achieve such goal: extraction and reassignment. In the following we will discuss these two ways in detail.

1) *Extracting transform*: The main idea of extracting transform is to present the TF coefficients consistent with the solutions of the IF equation, making the TF location concentrated and matching the IF or GD estimates.

Define an extractor as

$$\delta(\omega) = \begin{cases} 1, & \text{if } \omega = 0, \\ 0, & \text{if } \omega \neq 0, \end{cases} \quad (29)$$

then a concentrated TF representation is obtained by keeping only the TF points satisfying the IF equation, which is given by

$$T_e(t, \omega) = S_f^g(t, \omega) \delta(h_f(t, \omega)). \quad (30)$$

We refer to (30) as the extracting transform. This transform presents the oscillation content of the studied signal by detecting the solutions of the IF equation, retaining a small part of the TF coefficients of STFT and thus greatly sharpening the energy distribution.

The popular synchroextracting transform (SET) [39] can be considered a specialization of the extracting transform. Indeed, from expression (12), it is easy to get:

$$\hat{\omega}_1(t, \omega) = \Re \left\{ \frac{\partial_t S_f^g(t, \omega)}{j S_f^g(t, \omega)} \right\} = \phi'(t) + \frac{\sigma^4 c^2 (\omega - \phi'(t))}{1 + \sigma^4 c^2}. \quad (31)$$

Expression (31) indicates that the set of points  $\omega = \phi'(t)$  satisfies

$$\omega - \hat{\omega}_1(t, \omega) = 0. \quad (32)$$

Thus, equation (32) is a specific IF equation of chirp for  $(t, \omega) \in \Omega$ . Based on equation (32), it is easy to define the extracting transform as

$$T_e(t, \omega) = S_f^g(t, \omega) \delta(\omega - \hat{\omega}_1(t, \omega)), \quad (33)$$

which corresponds to the SET given in [39].

It is known that the extracting transform is not a type of energy conservation because they only retain the signal energy on the TF curves satisfying the IF equation, which brings a challenge to reconstruct the original signal. Based on equation (12) and the fact that

$$T_e(t, \phi'(t)) = S_f^g(t, \phi'(t)), \quad (34)$$

where  $\phi'(t)$  is the IF and generally estimated by the ridge of the extracting transform in terms of the locally maximal curve of  $|T_e(t, \omega)|$ , one can recover the harmonic-like signals from the extracting transform accurately. However, the reconstruction performance degrades when recovering the fast-varying signals [49]. Many improvements, such as the SECT [49] and adaptive signal separation operation (ASSO) [55], are proposed to derive a more accurate component recovery formula.

Another important problem for extracting transform is its numerical implementation, which should robustly remove the non-information TF points concerning the TF energy diffusion

and the noise. The numerical implementation of the extracting transform is frequently expressed as

$$T_e[m, n] = \begin{cases} S_f^g[m, n], & |h_f[m, n]| < \frac{\Delta\omega}{2}, |S_f^g[m, n]| > \lambda, \\ 0, & \text{otherwise,} \end{cases} \quad (35)$$

where  $S_f^g[m, n]$  and  $h_f[m, n]$  denote the discrete STFT and IF equation of the sampled signal respectively, and  $\Delta\omega$  is the discrete frequency interval. Except for this way, it is interesting to consider the nonlinear transformation of  $h_f$ , such as  $\exp(h_f) - 1$ , to obtain a more robust implementation.

2) *TF reassignment based on iterative algorithm*: Another way to sharpen the spread TF distribution is to move the TF values towards the IF or GD curves. Since the IFs or GDs of the studied signal  $f(t)$  are the solutions of the given IF equation  $h_f(t, \omega) = 0$ , i.e., the roots of  $h_f(t, \omega)$ , then for any  $(t, \omega) \in \Omega$ , we can consider it as an initial point of a numerical algorithm to solve a root of  $h_f(t, \omega)$ . When the numerical algorithm converges to the solutions of the IF equation with increasing iteration times, the spreading TF energy can be relocated to the instantaneous curves of the studied signal.

There are in fact many algorithms, such as the fixed point algorithm, the Newton algorithm, and the Levenberg-Marquardt (LM) algorithm [55] can be used to obtain a solution of that

$$h_f(t, \omega) = 0. \quad (36)$$

Specifically, starting with an arbitrary initial point  $(t, \omega_0) \in \Omega$ , the fixed point algorithm yields the iteration with respect to variable  $\omega$  that

$$\omega_{k+1} = \omega_k + \tau h_f(t, \omega_k), \quad (37)$$

where  $k = 0, 1, 2, \dots$ , and  $\tau \neq 0$  is hoped to converge to a root of  $h_f$ . Suppose the iteration of (37) is convergent to  $\omega^*$ , a root of the IF equation and a function of  $(t, \omega_0)$ , then we have

$$h_f(t, \omega^*) = 0.$$

To show the TF content of the signal more accurately and with better readability, we reassign the TF value of  $(t, \omega_0)$  to the location  $(t, \omega^*)$  as follows:

$$T_r(t, \omega^*) := S_f^g(t, \omega_0) + S_f^g(t, \omega^*). \quad (38)$$

Similar to the expression (9) in the SST, this reassignment operation above can be formulated as

$$T_r(t, \omega) = \int_{|S_f^g(t, \eta)| > \lambda} S_f^g(t, \eta) \delta(\omega - \omega^*(t, \eta)) d\eta. \quad (39)$$

Due to the relocation of the TF points only along the frequency direction, the original signal can be approximated by

$$f(t) \approx \frac{1}{g(0)} \int T_r(t, \omega) d\omega. \quad (40)$$

In the following, we utilize two concrete IF equations, i.e., the  $IF_1$  and  $IF_2$  of the chirps, to discuss the convergence of

the fixed point algorithm (37). For the  $IF_1$ , the iteration of  $\omega$  at time  $t$  can be expressed as

$$\omega_{k+1} = \omega_k + \tau \left| \frac{\frac{\partial}{\partial \omega} S_f^g(t, \omega)|_{\omega=\omega_k}}{S_f^g(t, \omega_k)} \right|^2 = \omega_k + \tau \frac{\sigma^4 (\omega_k - \phi'(t))^2}{1 + \sigma^4 c^2}. \quad (41)$$

Expression (41) yields that

$$\begin{aligned} & |\omega_{k+1} - \omega_k| \\ &= \left| \omega_k - \omega_{k-1} + \frac{\tau \sigma^4}{1 + \sigma^4 c^2} ((\omega_k - \phi'(t))^2 - (\omega_{k-1} - \phi'(t))^2) \right| \\ &\leq \left| 1 + \frac{\tau \sigma^4}{1 + \sigma^4 c^2} (\omega_k + \omega_{k-1} - 2\phi'(t)) \right| |\omega_k - \omega_{k-1}|. \end{aligned} \quad (42)$$

The parameter  $\tau$  can be set as  $0 < \tau < \frac{1+\sigma^4 c^2}{\sigma^4 \tilde{\Delta}}$  if the initial point satisfies  $\omega_0 < \phi'(t)$ , and set as  $-\frac{1+\sigma^4 c^2}{\sigma^4 \tilde{\Delta}} < \tau < 0$  if the initial point satisfies  $\omega_0 > \phi'(t)$ , to ensure the convergence. Here  $\tilde{\Delta}$  denotes the support of  $e^{-\frac{\sigma^2}{2(1+\sigma^4 c^2)} \omega^2}$ .

When considering the  $IF_2$ , the iteration of (37) can be further written as

$$\omega_{k+1} = \omega_k + \tau \Re \left\{ \frac{\frac{\partial}{\partial \omega} S_f^g(t, \omega)|_{\omega=\omega_k}}{S_f^g(t, \omega_k)} \right\} = \omega_k - \tau \frac{\sigma^2 (\omega_k - \phi'(t))}{1 + \sigma^4 c^2}, \quad \omega_{k+1} = \omega_k - \frac{1}{2 \left( \Re \left\{ \frac{-j S_f^{t^2 g}(t, \omega_k)}{S_f^{t g}(t, \omega_k)} \right\} - \Re \left\{ \frac{-j S_f^{t g}(t, \omega_k)}{S_f^g(t, \omega_k)} \right\} \right)}. \quad (43)$$

From (43), we have

$$\begin{aligned} & |\omega_{k+1} - \omega_k| \\ &= \left| \omega_k - \omega_{k-1} - \frac{\tau \sigma^2}{1 + \sigma^4 c^2} (\omega_k - \phi'(t) - (\omega_{k-1} - \phi'(t))) \right| \\ &\leq \left| 1 - \frac{\tau \sigma^2}{1 + \sigma^4 c^2} \right| |\omega_k - \omega_{k-1}|. \end{aligned} \quad (44)$$

Therefore, iteration (43) is convergent if  $\tau$  is taken as a value such that  $|1 - \frac{\tau \sigma^2}{1 + \sigma^4 c^2}| < 1$ .

It should be pointed out that the multi-synchrosqueezing transform [44] is a specific case of the IF equation-based reassignment method. Indeed, when we consider the IF equation (32) and take the value of  $\tau$  in (37) as -1, then iteration (37) can be written as

$$\omega_{k+1} = \hat{\omega}_1(t, \omega_k), \quad k = 0, 1, 2, \dots, \quad (45)$$

which corresponds to the multiple SST operation in [44]. Beyond this specific case, we can consider selecting another value of  $\tau$  in (37) to further improve the convergence.

Moreover, we can also use the Newton algorithm to get a root of  $h_f(t, \omega)$ . For the initial point  $(t, \omega_0)$  in  $\Omega$ , the Newton iteration formula can be expressed as

$$\omega_{k+1} = \omega_k - \frac{h_f(t, \omega_k)}{\frac{\partial}{\partial \omega} h_f(t, \omega)|_{\omega=\omega_k}}, \quad k = 0, 1, 2, \dots \quad (46)$$

Specifically, with regard to the case of the  $IF_1$  of chirp signals, Newton iteration (46) can be further written as

$$\omega_{k+1} = \frac{1}{2} (\omega_k + \phi'(t)), \quad (47)$$

which leads to

$$|\omega_{k+1} - \omega_k| = \frac{1}{2} |\omega_k - \omega_{k-1}|.$$

It is easy to prove that the Newton iteration used for solving the IF equation  $IF_1$  is convergent.

Due to that

$$h_f(t, \omega) = \left| \frac{\frac{\partial}{\partial \omega} S_f^g(t, \omega)}{S_f^g(t, \omega)} \right|^2, \quad \text{for } (t, \omega) \in \Omega,$$

we have

$$\begin{aligned} \frac{h_f(t, \omega)}{\frac{\partial}{\partial \omega} h_f(t, \omega)} &= \frac{\left| \frac{\partial}{\partial \omega} S_f^g(t, \omega) \right| |S_f^g(t, \omega)|}{2 \left( \frac{\partial}{\partial \omega} \left| \frac{\partial}{\partial \omega} S_f^g(t, \omega) \right| |S_f^g(t, \omega)| - \frac{\partial}{\partial \omega} |S_f^g(t, \omega)| \left| \frac{\partial}{\partial \omega} S_f^g(t, \omega) \right| \right)}. \end{aligned} \quad (48)$$

Since  $\left| \frac{\partial}{\partial \omega} S_f^g(t, \omega) \right| = \left| S_f^{t g}(t, \omega) \right|$ ,  $\frac{\partial}{\partial \omega} |S_f^g(t, \omega)| = \Re \left\{ \frac{-j S_f^{t g}(t, \omega)}{S_f^g(t, \omega)} \right\} |S_f^g(t, \omega)|$ , and  $\frac{\partial}{\partial \omega} \left| \frac{\partial}{\partial \omega} S_f^g(t, \omega) \right| = \Re \left\{ \frac{-j S_f^{t^2 g}(t, \omega)}{S_f^{t g}(t, \omega)} \right\} |S_f^{t g}(t, \omega)|$ , then the Newton iteration can be more efficiently computed by

$$\omega_{k+1} = \omega_k - \frac{1}{2 \left( \Re \left\{ \frac{-j S_f^{t^2 g}(t, \omega_k)}{S_f^{t g}(t, \omega_k)} \right\} - \Re \left\{ \frac{-j S_f^{t g}(t, \omega_k)}{S_f^g(t, \omega_k)} \right\} \right)}. \quad (49)$$

In order to improve the convergence of the Newton algorithm when used for  $IF_1$ , we can reformulate (46) as

$$\omega_{k+1} = \omega_k - 2 \frac{h_f(t, \omega_k)}{\frac{\partial}{\partial \omega} h_f(t, \omega)|_{\omega=\omega_k}}. \quad (50)$$

One iteration of (50) can converge to the solution of the IF equation of chirps. Therefore, developing an effective iterative algorithm is another powerful way to obtain a concentrated TF distribution, compared with the IF estimator.

It is noted that the reassignment operation along the frequency direction is not sufficient for GD characterization when addressing the mixed signals. Future works will consider new reassignment operations with an adaptive pattern to yield a high-accuracy TF description.

## D. Comparison

This section uses a simulated example to test the performance of the IF equation-based TF post-processing methods and compare them with the IF estimator-based TF post-processing methods.

The waveform of the test signal is illustrated in Fig. 1(a), which contains two impulsive signals, a chirp, and a cosine modulation component. We compute the TF representations of the signal using the FSST [24], second-order SST (SSST for short) [42], time-reassigned SST (TSST for short) [46], extracting transform based on  $IF_i$  (ETIF<sub>*i*</sub> for short,  $i = 1, 2, 3$ ), reassignment method based on the Newton iteration and  $IF_1$  (RMNIF<sub>1</sub> for short), and reassignment method based on the fixed point algorithm and  $IF_2$  (RMFPIF<sub>2</sub> for short). From the results, we can observe that the FSST and SSST yield good energy concentration for the chirp and cosine-modulated signal but fail to characterize the impulsive signals effectively.

The TSST provides a better TF localization for the transient signals while degrading the TF sharpness of the stationary mode. For our introduced extracting transforms, the  $\text{ETIF}_1$  provides excellent performance in dealing with the mixed signal;  $\text{ETIF}_2$  provides a high-concentration TF representation for the chirp and the cosine modulation signal but results in a blurred TF representation for impulsive signals;  $\text{ETIF}_3$  leads to the opposite result compared with  $\text{ETIF}_2$ . The results imply the fact that the IF equation  $IF_2$  is more suitable for characterizing the time-varying signals, like chirps and cosine modulation signals, whereas the  $IF_3$  is more useful in detecting the impulsive signals. The  $\text{RMNIF}_1$  and  $\text{RMFPIF}_2$  have better TF plots than FSST and achieve competitive results

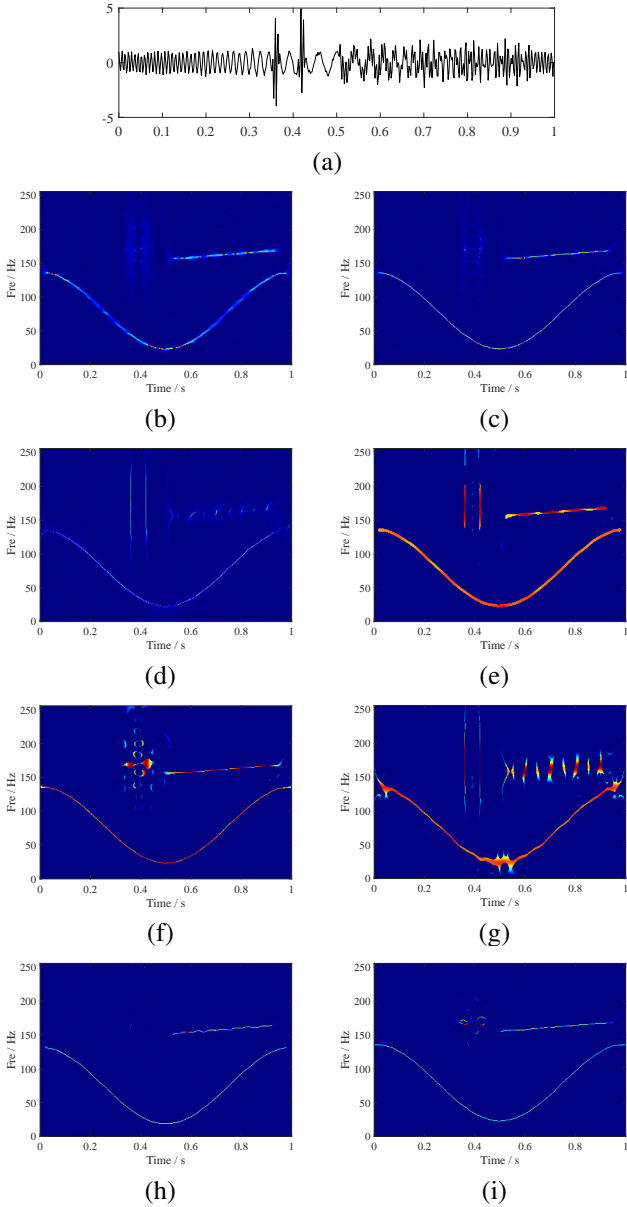


Fig. 1: Evaluation of TF results on a known signal structure. (a) Waveform of the test signal, (b) TF plot by FSST, (c) TF plot by SSST, (d) TF plot by TSST, (e) TF plot by  $\text{ETIF}_1$ , (f) TF plot by  $\text{ETIF}_2$ , (g) TF plot by  $\text{ETIF}_3$ , (h) TF plot by  $\text{RMNIF}_1$ , (i) TF plot by  $\text{RMFPIF}_2$ .

with the SSST. Unfortunately, all of the reassignment methods considered here lead to the blurred characterization of the impulsive signals because of the limitation of the reassignment operation along the frequency direction, as shown in Fig. 1(b, c, h, i). In this regard, the extracting transform appears to be more effective.

Although the  $\text{ETIF}_1$  shows excellent potential in handling the mixed signal, there still exist two issues to be addressed. First,  $\text{ETIF}_1$  does not achieve an ideal energy concentration, still resulting in TF representation diffusion because Rényi entropy of the TF representation by  $\text{ETIF}_1$  is 11.52, larger than the values by SSST (11.17) and  $\text{ETIF}_2$  (10.88). Second, it is subject to the extracting operation and the function of the IF equation, sometimes leading to discontinuous TF information curves when pursuing a high-concentration TF representation. Fig. 2(a) displays the TF result of  $\text{ETIF}_1$  when using a relatively small threshold value in (35). Obviously, the disconnected characterization of the chirp occurs in the TF plot, as marked with the pink box.

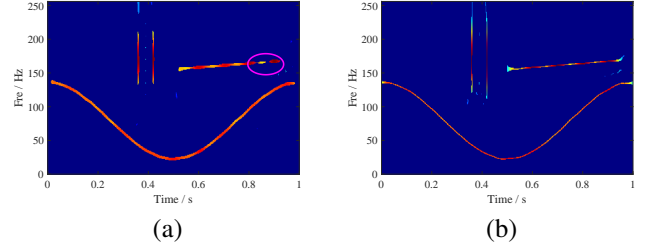


Fig. 2: Evaluation of TF results on a known signal structure. (a) TF plot by  $\text{ETIF}_1$ , (b) TF plot by ETCIFLS.

#### IV. COMBINATION OF IF EQUATIONS BASED ON LOCAL SPARSITY

To address the two issues above, this section introduces a novel approach to combine different IF equations to minimize energy spreading based on local sparsity.

From the analysis in the previous section, we know that the  $IF_2$  provides a high-concentration TF representation for time-varying signals. Namely, it guarantees the sparsity of the TF distribution when characterizing time-varying signals. Alternatively, the  $IF_3$  leads to a sparse TF representation for frequency-varying signals. The attempt is to select the sparser representation from the TF distributions using the two IF equations, i.e.,  $IF_2$  and  $IF_3$ .

We here consider a discrete signal with  $N$  samples and suppose  $IF_2$  and  $IF_3$  be known, which leads to two TF representations of  $\text{ETIF}_2 \in \mathbb{C}^{M \times N}$  and  $\text{ETIF}_3 \in \mathbb{C}^{M \times N}$ . For each TF bin  $(m, n)$ , a local TF representation performed by a two-dimensional window  $W_s$  with  $(2n_w + 1) \times (2n_w + 1)$  elements can be obtained that

$$\widetilde{\text{ETIF}}_i^{m,n} := \widetilde{\text{ETIF}}_i[m - n_w : m + n_w, n - n_w : n + n_w] \circledast W_s, \quad (51)$$

where  $\widetilde{\text{ETIF}}_i \in \mathbb{C}^{(M+2n_w) \times (N+2n_w)}$  is the extension of  $\text{ETIF}_i$  by zero padding,  $i = 2, 3$ ,  $m = n_w + 1, n_w + 2, \dots, n_w + M$ ,  $n = n_w + 1, n_w + 2, \dots, n_w + N$ , and  $\circledast$  denotes the element-

wise product. The sparsity of each TF region  $\widetilde{\text{ETIF}}_i^{m,n}$  is then measured via calculating the Gini index [58] as

$$G(X) = 1 - 2 \sum_{i=1}^{N_s} \frac{x_i}{\|\vec{x}\|_1} \left( \frac{N_s - i + \frac{1}{2}}{N_s} \right), \quad (52)$$

where  $\vec{x} = [x_1 \ x_2 \ \cdots \ x_{N_s}]$  containing the elements of the magnitude of the input matrix  $X$  in ascending order, and  $\|\vec{x}\|_1$  denotes the  $l_1$ -norm of vector  $\vec{x}$ . The value of the Gini index is limited to the interval  $[0, 1]$ , where the value near 0 denotes a group of samples with equally distributed energy and near 1 means maximum energy concentration.

After computing the local sparsity of all local representations using  $IF_2$  and  $IF_3$ , a TF representation is constructed to indicate which exhibits the highest local sparsity for each TF bin:

$$\text{ETCIFLS}[m, n] := \text{ETIF}_p[m, n], \quad (53)$$

where  $p = \max_i G(\widetilde{\text{ETIF}}_i^{m,n})$ . This representation is a combination of extracting transform with different IF equations and is an optimum representation in terms of local sparsity. We denote it as ETCIFLS.

Fig. 2(b) depicts the TF representation of the test signal in Fig. 1(a) using ETCIFLS. Rényi entropies of the two TF representations in Fig. 2 are computed as 11.69 (ETIF<sub>1</sub>) and 10.79 (ETCIFLS). The experimental results show that the energy concentration of ETCIFLS is greatly improved compared to that of the ETIF<sub>1</sub>, and ETCIFLS provides more detailed and accurate TF information than ETIF<sub>1</sub>.

It is worth noting that a disadvantage of this method, in comparison to the approach presented in the previous section, is that the ETCIFLS requires much higher computational resources because it involves not only the STFT calculations with different windows but also the local sparsity detections. When considering the signal of  $N$  samples, the STFT can be implemented by the FFT, which requires  $O(N^2 \log_2 N)$  operations, and the sparsity measure requires  $O(N^2(2n_w + 1)^2)$  computations. Therefore, the total computing complexity of ETCIFLS is  $O(N^2(\log_2 N + (2n_w + 1)^2))$ , in which, a large one of  $n_w$  inevitably leads to an increase in time cost.

The window  $W_s$ , responsible for the local sparsity computation, is designed as a two-dimensional Hamming window. The dimensions of  $W_s$  are related to the resolutions of ETIF<sub>1</sub> and ETIF<sub>2</sub>. A large size generally increases the computation, whereas a small size easily results in a lack of TF information. Through experiments, we suggest the value of  $n_w$  of  $W_s$  can be considered as [10, 35], which leaves this window enough room for including the frequency components present in all TF representations and usually produces a satisfactory result.

## V. NUMERICAL VALIDATION

In this section, we conduct numerical simulations to illustrate the effectiveness of the proposed methods. For comparison, the state-of-the-art highly concentrated schemes, namely the SET [39], the SSST [42], the second-order synchroextracting wavelet transform (SSEWT for short) [7], and the MDD [59] have been used.

### A. Simulated signal

We first use the proposed methods to detect a mixed signal composed of three harmonic-like components and two impulsive-like components, which is given by

$$\begin{aligned} f(t) &= f_1(t) + f_2(t) + f_3(t) + f_4(t) + f_5(t) + n(t), \\ f_1(t) &= \sin(40\pi t), \quad t \in [0.33, 1.4], \\ f_2(t) &= \sin(80\pi t), \quad t \in [0.33, 1.4], \\ f_3(t) &= \sin(120\pi t + \pi t^2), \quad t \in [0.33, 1.4], \\ f_4(t) &= \Re\{FT(0.02 \exp(40\pi j t))\}, \quad t \in [0, 2], \\ f_5(t) &= \Re\{FT(0.02 \exp(70\pi j t))\}, \quad t \in [0, 2], \end{aligned} \quad (54)$$

where  $n(t)$  is the Gaussian noise with the SNR = 6 dB, and  $FT$  denotes the Fourier transform. The sampling frequency is 256 Hz.

Fig. 3 shows the TF representations obtained by the SET, SSST, SSEWT, MDD, ETIF<sub>1</sub>, and ETCIFLS. It can be seen from the results that, the SET and SSST give clear TF representations for  $f_1(t)$ ,  $f_2(t)$ , and  $f_3(t)$ , but fail to localize the other two impulsive components effectively. In contrast, the SSEWT can produce a concentrated TF representation for the transient signals but provides erroneous TF content for the harmonic models. The TF representation by MDD is blurred and there are heavy cross-terms between the neighboring modes in the TF plane. The ETIF<sub>1</sub> and ETCIFLS are superior to others, yielding good characterization of both time-varying harmonic and frequency-varying harmonic components. It should be noted that ETIF<sub>1</sub> gives discontinuous TF ridges, and misses a small amount of boundary information when pursuing a high-concentration TF representation. To show the performance of the proposed approaches quantitatively, we compute the time cost and Rényi entropy (RE) of the six TF analysis methods. The tested computer configuration is as follows: Intel Core i9-11900KF 3.50 GHz, 32.0 GB of RAM, and MATLAB version R2021a. As presented in Table I, the SSEWT and ETCIFLS have smaller values of RE among all the selected TF representations, so they have better energy concentration. The ETIF<sub>1</sub> takes less time than SSST and MDD to represent the signal. The ETCIFLS is relatively more time-consuming than the others to produce the result.

TABLE I: Performance comparison of the selected TF representations for signal (54).

Method	SET	SSST	SSEWT	MDD	ETIF <sub>1</sub>	ETCIFLS
Time (s)	0.041	0.219	0.062	0.268	0.035	5.951
RE	12.417	12.707	11.115	16.596	13.037	11.520

We next consider a four-component AM-FM signal including a signal with hyperbolic frequency modulation, a cosine modulation signal, and two impulse components, that is

$$\begin{aligned} f(t) &= f_1(t) + f_2(t) + f_3(t) + f_4(t) + n(t), \\ f_1(t) &= \cos(20\pi(15t + 5 \log(|t|))), \quad t \in (0, 1], \\ f_2(t) &= (1.2 + 0.1 \sin(10\pi t)) \sin(2\pi(145t - 4 \times \\ &\quad \exp(-0.3t + 0.4) \sin(6\pi(t2 - 0.2))))), \quad t \in [0.2, 0.5], \\ f_3(t) &= 5 \exp(-10000\pi(t - 0.74)^2) \cos(280\pi t), \quad t \in [0, 1], \\ f_4(t) &= 5 \exp(-10000\pi(t - 0.8)^2) \cos(280\pi t), \quad t \in [0, 1], \end{aligned} \quad (55)$$

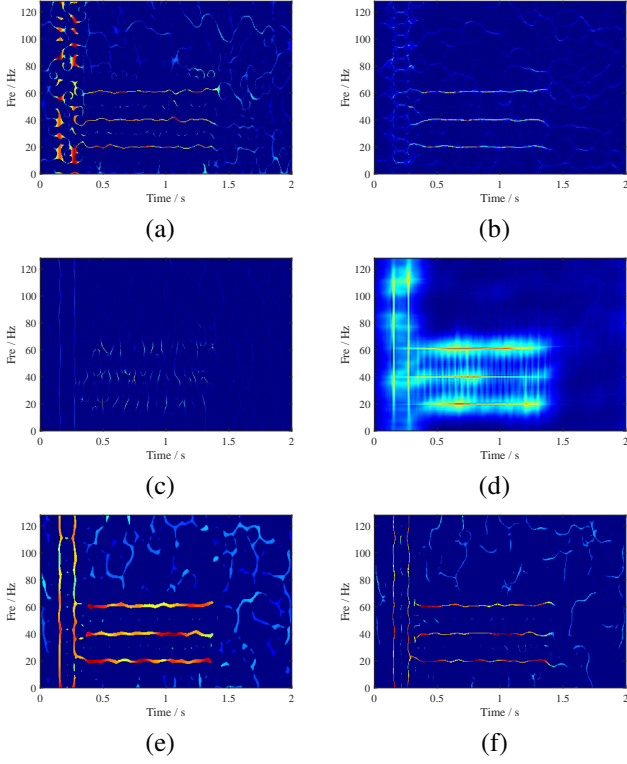


Fig. 3: TF results of signal (54) using various analysis methods. (a) SET, (b) SSST, (c) SSEWT, (d) MDD (1, 0.003), (e) ETIF<sub>1</sub>, (f) ETCIFLS ( $n_w = 41$ ).

where  $n(t)$  is the Gaussian noise with the SNR= 5 dB. The sampling frequency is 512 Hz.

The TF representations of the test signal (55) using the six TF methods are provided in Fig. 4. The results show SET and SSST are ineffective in characterizing the impulsive-like models, from which, it is easy to recognize some signal information as noise. The SSEWT provides a better TF localization for the transient signals while degrading the TF sharpness of the stationary part of the hyperbolic signals (see TF plot in the time interval [0.2, 1]). As given in Fig. 4(d), the MDD has a blurred TF representation, from which it is difficult to identify and separate. From Fig. 4(e) and (f), it can be seen that ETIF<sub>1</sub> and ETCIFLS improve the energy concentration highly, and IF trajectories of all components of the mixed signal can be identified. Moreover, the ETCIFLS has better TF concentration and continuity with less noise interference compared with ETIF<sub>1</sub>.

TABLE II: Performance comparison of the six TF representations for signal (55).

Method	SET	SSST	SSEWT	MDD	ETIF <sub>1</sub>	ETCIFLS
Time (s)	0.030	0.207	0.043	0.274	0.176	2.588
RE	11.485	12.257	10.291	15.232	12.690	11.068

Table II provides the quantitative results of the employed methods. It can be observed that the first five methods are more efficient in computation. The ETCIFLS gives an accurate TF description and has better TF concentration than SET, SSST, MDD, and ETIF<sub>1</sub>.

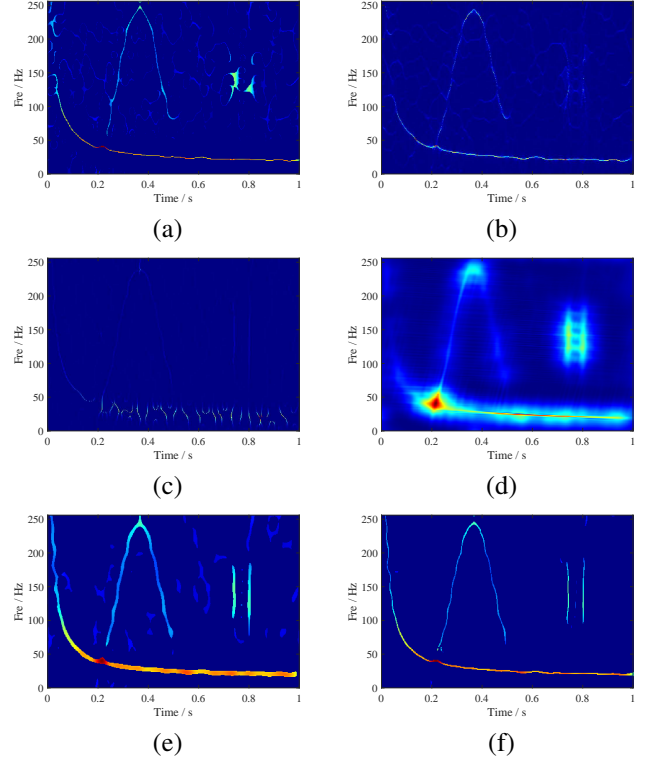


Fig. 4: TF results of signal (55) using various analysis methods. (a) SET, (b) SSST, (c) SSEWT, (d) MDD (1, 0.003), (e) ETIF<sub>1</sub>, (f) ETCIFLS ( $n_w = 41$ ).

### B. IF detection under different noise levels

In order to explore the performance of the proposed approaches in IF characterization and noise robustness, we give the IF estimates of a multi-component signal under different SNRs of noise. The IF trajectories of the signal are detected by linking the peak data from the TF representation, as used in [44,49]. The test signal model is defined as:

$$\begin{aligned}
 f(t) &= f_1(t) + f_2(t) + n(t), \quad t \in [0, 3], \\
 f_1(t) &= 0.5 \exp(-0.01t) \cos(2\pi(225t - 7(t - 0.8)^3 + 5t^2)), \\
 f_2(t) &= \sin(2\pi(90t + 14 \arctan((5t^2 - 2)^2))),
 \end{aligned} \tag{56}$$

where  $n(t)$  denotes the Gaussian white noise. The sampling frequency is 512 Hz.

Fig. 5 shows the logarithmic mean square error (MSE) between the true and estimated IF under different SNRs by performing 100 simulations. The SSEWT fails to produce correct IF approximates of the test signal (56). The MDD shows good noise robustness at SNRs less than 0 dB but fails to improve the accuracy at higher SNRs. The SET and SSST give better representation for  $f_1(t)$  than  $f_2(t)$ , and the SSST has better performance than SET in dealing with  $f_1(t)$ . The ETIF<sub>1</sub> is comparable to the performance of SST and SSST at low SNRs (SNR < 0 dB) and generally, shows better noise robustness than ETCIFLS. Both ETIF<sub>1</sub> and ETCIFLS achieve better performance than other methods when addressing the mode  $f_2(t)$  at SNRs greater than 2 dB. The comparison result indicates the effectiveness of the proposed methods in characterizing signals (56), especially under high SNR. The

noise robustness of ETCIFLS and more effective IF detection algorithms should be explored in later research.

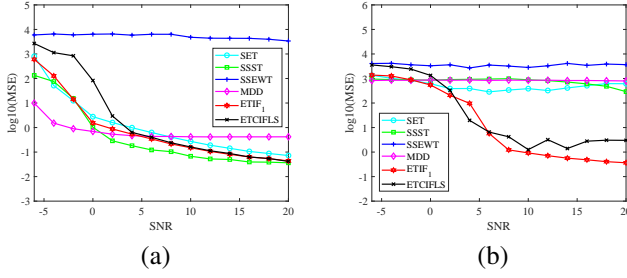


Fig. 5: MSE of the IF estimates of signal (56) under different noise interference. (a) MSE of the IF estimate of  $f_1(t)$ , (b) MSE of the IF estimate of  $f_2(t)$ .

### C. Application to EEG Seizure Signal

In this subsection, we will investigate the applicability of the proposed approach for analyzing an epileptic EEG seizure signal [60]. This signal mainly includes two types of components, tones and spikes. The sampling frequency of the signal is 32 Hz and about 8 seconds of data is displayed in Fig. 6.

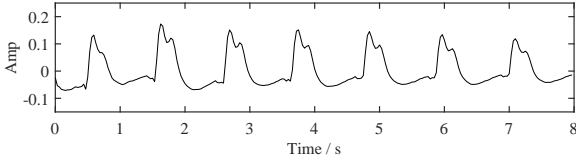


Fig. 6: The waveform of the epileptic EEG seizure signal.

Fig. 7 shows the corresponding TF representations associated with the STFT, SET, SSST, SSWET, MDD, and ETCIFLS. It can be seen that the STFT provides energy characterization for tones, giving blurred TF representation for spikes. Fig. 7(b) and (e) show that SET and MDD sharpen the TF distribution of the tones compared with the STFT, but still fail to resolve the spikes. The SSST (Fig. 7(c)) presents a blurry TF representation, based on which, it is difficult to make further analysis and judgment. The SSWET (Fig. 7(d)) concentrates the TF energy of the spikes while failing to show the TF information of the tones. Fig. 7(f) shows that the proposed ETCIFLS can identify both tones and spikes clearly in the TF plane, exhibiting great potential in EEG signal analysis.

### D. Application to Gravitational-wave Signal

The second practical signal is a gravitational-wave (GW) signal [61] generated by the merge of two stellar-mass black holes. This signal is a typical AM-FM signal and accompanied by large noise. The sampling frequency is 4096 and the time-series waveform of the signal is plotted in Fig. 8.

The instantaneous information of the GW signal contains significant features corresponding to the collision of two black holes, thus it is necessary to remove any additional spurious

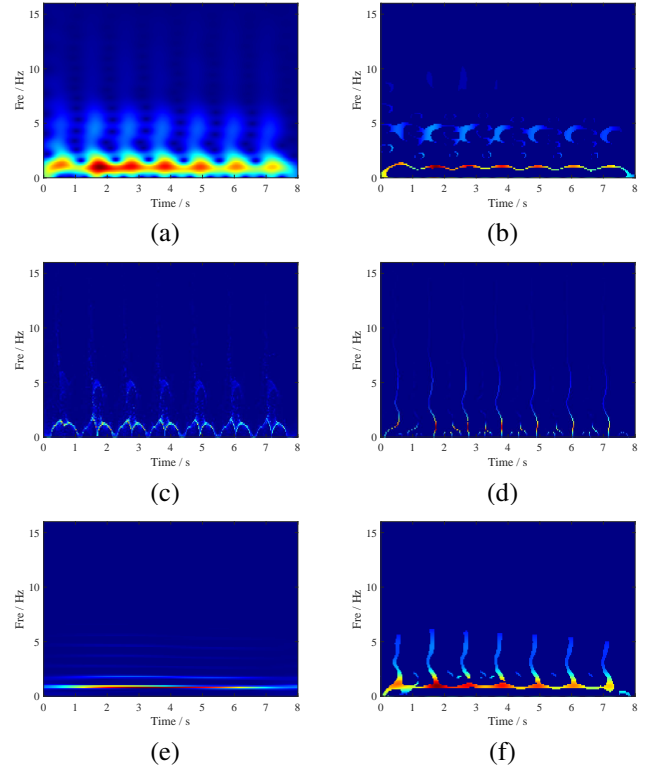


Fig. 7: TF representations of a real newborn EEG seizure signal composed of spikes and a pseudosinusoid. (a) TF plot by STFT, (b) TF plot by SET, (c) TF plot by SSST, (d) TF plot by SSWET, (e) TF plot by MDD (2, 0.05), (f) TF plot by ETCIFLS ( $n_w = 71$ ).

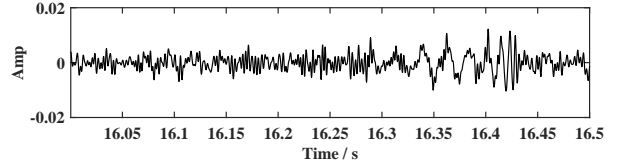


Fig. 8: Waveform of the gravitational-wave signal.

disturbance to obtain its accurately time-varying characteristics. Fig. 9 shows the TF representations of the GW signal by the six TF analysis methods. From the TF plot, we can see it 'chirping' from lower to higher frequency over a small fraction of a second, i.e., the hyperbolic-like frequency-modulation component indicated by a yellow box. For this component, the first three methods yield a spread or absent TF content for the fast-varying part, while SSWET provides a discontinuous TF curve for the harmonic-like part. The MDD can characterize the basic features of the GW signal. The ETCIFLS shows a good resolution on the TF representation of the hyperbolic-like component and effectively indicates the time of the incoming GW signal.

The IF estimates of the component at the area of time [16.3 16.45] are also given in the right half of Fig. 9. It can be seen from the results that the ETCIFLS provides a better characterization, based on which the IF information can be clearly identified. This case demonstrates the capability of ETCIFLS to detect the complex gravitational-wave signal and to generate high-concentration TF description in dealing with

hyperbolic-like signals.

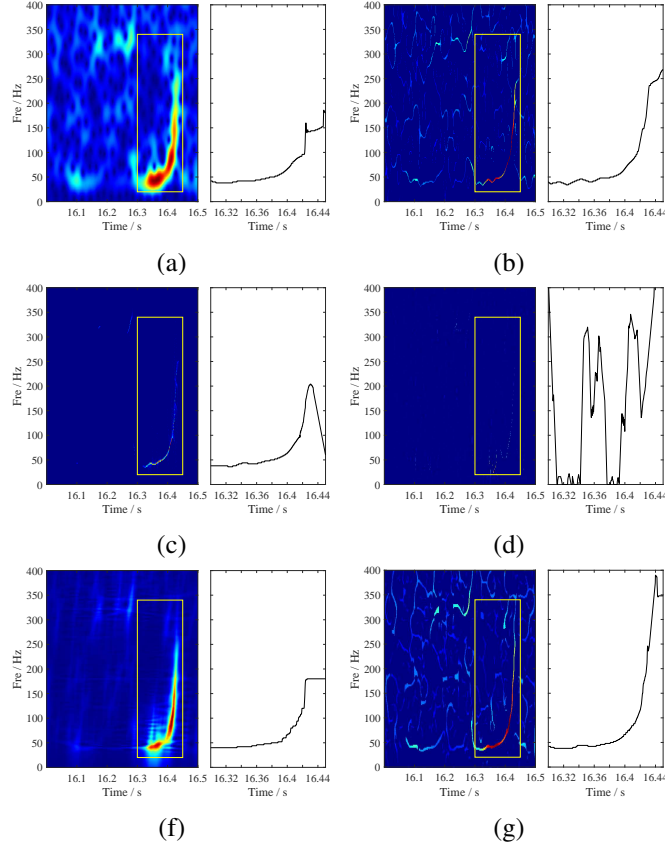


Fig. 9: TF results and IF estimation by various analysis methods. (a) STFT, (b) SET, (c) SSST, (d) SSEWT, (e) MDD (2, 0.05), (f) ETCIFLS ( $n_w = 51$ ).

## VI. CONCLUSION

In this paper, we discussed the IF equation-based TF analysis method to generate a concentrated TF representation for mixed signals. The IF equation we defined does serve as a feature extractor to characterize the slow-varying and fast-varying modes. Several properties of the IF equation were studied and proved theoretically. Based on the IF equation, we introduced two classical ways, that is, extraction and reassignment, to obtain a highly-concentrated TF output. The IF equation-based TF post-processing methods provide another way to improve the TF resolution and cover many popular TF analysis methods, such as the synchroextracting transform, the multi-synchrosqueezing transform, and the time extracting transform, etc. We also proposed combining different IF equations based on local information to preserve the best concentration of each representation. Several experiments on both synthetic and real-world signals showed that our approaches have better performance in dealing with a mixture of impulse-like signals, hyperbolic frequency modulation components, chirps, and cosine modulation signals.

We are going to share the corresponding code on the Matlab Central website soon, and the code is also available upon the request to the first author.

## REFERENCES

- [1] M.G. Amin, Y.D. Zhang, F. Ahmad, K. Ho, "Radar signal processing for elderly fall detection: The future for in-home monitoring", *IEEE Signal Process. Mag.*, vol. 33, no. 2, pp. 71-80, 2016.
- [2] A.A. Ahmad, S. Lawan, M. Ajiya, Z.Y. Yusuf, L. Bello, "Extraction of the pulse width and pulse repetition period of linear FM radar signal using time-frequency analysis", *Journal of Advances in Science and Engineering*, vol. 3, no. 1, pp. 1-8, 2020.
- [3] Y. Miao, J. Li, H. Sun, "Multimodal sparse time-frequency representation for underwater acoustic signals", *IEEE Journal of Oceanic Engineering*, vol. 46, no. 2, pp. 642-653, 2021.
- [4] P.M. Tripathi, A. Kumar, M. Kumar, R. Komaragiri, "Multilevel classification and detection of cardiac arrhythmias with high-resolution superlet transform and deep convolution neural network", *IEEE Trans. Instrum. Meas.*, vol. 71, pp. 1-13, 2022.
- [5] H-T. Wu, "Current state of nonlinear-type time-frequency analysis and applications to high-frequency biomedical signals", *Current Opinion in Systems Biology*, vol. 23, pp. 8-21, 2020.
- [6] J. Shi, J. Zheng, X. Liu, W. Xiang, Q. Zhang, "Novel short-time fractional Fourier transform: theory, implementation, and applications", *IEEE Trans. Signal Process.*, vol. 68, pp. 3280-3295, 2020.
- [7] B. Han, Y. Zhou, G. Yu, "Second-order synchroextracting wavelet transform for nonstationary signal analysis of rotating machinery", *Signal Process.*, vol. 186, 2022, no. 108123.
- [8] M.R. Portnoff, "Time-frequency representation of digital signals and systems based on short-time Fourier analysis", *IEEE Trans. Acoust. Speech Signal Process.*, vol. 28, no. 1, pp. 55-69, 1980.
- [9] A. Grossmann, J. Morlet, "Decomposition of hardy functions into square integrable wavelets of constant shape", *SIAM J. Math. Anal.*, vol. 15, no. 4, pp. 723-736, 1984.
- [10] R. Stockwell, L. Mansinha, R. Lowe, "Localization of the complex spectrum: the S transform", *IEEE Trans. Signal Process.*, vol. 44, no. 4, pp. 998-1001, 1996.
- [11] S. Mann, S. Haykin, "The chirplet transform: physical considerations," *IEEE Trans. Signal Process.*, vol. 43, no. 11, pp. 2745-2761, 1995.
- [12] L. Cohen, *Time-Frequency Analysis*, Prentice-Hall, Englewood Cliffs, NJ, 1995.
- [13] K. Kodera, R. Gendrin, C. Villedary, "Analysis of time-varying signals with small BT values", *IEEE Trans. Acoust. Speech Signal Process.*, vol. 26, pp. 64-76, 1978.
- [14] F. Auger, P. Flandrin, "Improving the readability of time-frequency and time-scale representations by the reassignment method", *IEEE Trans. Signal Process.*, vol. 43, no. 5, pp. 1068-1089, 1995.
- [15] F. Auger, E. Chassande-Mottin, P. Flandrin, "Making reassignment adjustable: the Levenberg-Marquardt approach", *2012 IEEE International Conference on Acoustics, Speech and Signal Processing*, Kyoto, Japan, 2012, pp. 3889-3892.
- [16] J. Xiao, P. Flandrin, "Multitaper time-frequency reassignment for nonstationary spectrum estimation and chirp enhancement", *IEEE Trans. Signal Process.*, vol. 55, no. 6, pp. 2851-2860, 2007.
- [17] V. Bruni, M. Tartaglione, D. Vitulano, "An iterative approach for spectrogram reassignment of frequency modulated multicomponent signals", *Math. Comput. Simulat.*, vol. 176, pp. 96-119, 2020.
- [18] I. Reinhold, M. Sandsten, "The multitaper reassigned spectrogram for oscillating transients with Gaussian envelopes", *Signal Process.*, vol. 198, 2022, no. 108570.
- [19] D. Wei, Z. Huang, H. Mao, X. Li, H. Huang, B. Wang, X. Yi, "Iterative reassignment: An energy-concentrated time-frequency analysis method", *Mech. Syst. Signal Process.*, vol. 182, 2023, no. 109579.
- [20] S. Meignen, T. Oberlin, D.H. Pham, "Synchrosqueezing transforms: From low- to high-frequency modulations and perspectives", *C. R. Phys.*, vol. 20, pp. 449-460, 2019.
- [21] I. Daubechies, S. Maes, "A nonlinear squeezing of the continuous wavelet transform based on auditory nerve models", in: *Wavelets in Medicine and Biology*, CRC Press, 1996, pp. 527-546.
- [22] I. Daubechies, J.F. Lu, H.T. Wu, "Synchrosqueezed wavelet transforms: an empirical mode decomposition-like tool", *Appl. Computat. Harmon. Anal.*, vol. 30, pp. 243-261, 2011.
- [23] N.E. Huang, Z. Shen, S.R. Long, M. Wu, H. Shih, Q. Zheng, N. Yen, C. Tung, H. Liu, "The empirical mode decomposition and Hilbert spectrum for nonlinear and nonstationary time series analysis", *Proc. R. Soc. Lond. A*, vol. 454, pp. 903-995, 1998.
- [24] G. Thakur, H.T. Wu, "Synchrosqueezing-based recovery of instantaneous frequency from nonuniform samples", *SIAM J. Math. Anal.*, vol. 43, no. 5, pp. 2078-2095, 2012.

- [25] H. Yang, "Synchrosqueezed wave packet transforms and diffeomorphism based spectral analysis for 1D general mode decompositions", *Appl. Comput. Harmon. Anal.*, vol. 39, no. 1, pp. 33-66, 2015.
- [26] H. Yang, L. Ying, "Synchrosqueezed curvelet transform for two dimensional mode decomposition", *SIAM. J. Math. Anal.*, vol. 46, no. 3, pp. 2052-2083, 2014.
- [27] Z. Huang, J. Zhang, Z. Zou, "Synchrosqueezing S-transform and its application in seismic spectral decomposition", *IEEE Trans. Geosci. Remote Sens.*, vol. 54, no. 2, pp. 817-825, 2016.
- [28] N. Liu, J. Gao, Z. Zhang, X. Jiang, Q. Lv, "High resolution characterization of geological structures using synchrosqueezing transform", *Interpretation*, vol. 5, no. 1, pp. T75-T85, 2017.
- [29] D. Wei, J. Shen, "Multi-spectra synchrosqueezing transform", *Signal Process.*, vol. 207, 2023, no. 108940.
- [30] G. Thakur, E. Brevdo, N.S. Fućkar, H.T. Wu, "The Synchrosqueezing algorithm for time-varying spectral analysis: robustness properties and new paleoclimate applications", *Signal Process.*, vol. 93, pp. 1079-1094, 2013.
- [31] I. Daubechies, Y. Wang, H.T. Wu, "ConceFT: concentration of frequency and time via a multitapered synchrosqueezed transform", *Philos. Trans. R. Soc.*, vol. 374, 2016, no. 20150193.
- [32] H. Yang, "Statistical analysis of synchrosqueezed transforms", *Appl. Comput. Harmon. Anal.*, vol. 45, no. 3, pp. 526-550, 2018.
- [33] Z.C. Zhang, T. Yu, M.K. Luo, K. Deng, "Estimating instantaneous frequency based on phase derivative and linear canonical transform with optimised computational speed", *IET Signal Proc.*, vol. 12, no. 5, pp. 574-580, 2018.
- [34] A. Ahrabian, D. Looney, L. Stanković, D.P. Mandic, "Synchrosqueezing-based time-frequency analysis of multivariate data", *Signal Process.*, vol. 106, pp. 331-341, 2015.
- [35] L. Li, H. Cai, H. Han, Q. Jiang, H. Ji, "Adaptive short-time Fourier transform and synchrosqueezing transform for non-stationary signal separation", *Signal Process.*, vol. 66, 2020, no. 107231.
- [36] L. Li, H.Y. Cai, Q.T. Jiang, "Adaptive synchrosqueezing transform with a time-varying parameter for non-stationary signal separation", *Appl. Comput. Harmon. Anal.*, vol. 49, pp. 1075-1106, 2020.
- [37] J. Lu, Q. Jiang, L. Li, "Analysis of adaptive synchrosqueezing transform with a time-varying parameter", *Adv Comput Math*, vol. 46, 2020, no. 72.
- [38] H.Y. Cai, Q.T. Jiang, L. Li, B.W. Suter, "Analysis of adaptive short-time Fourier transform-based synchrosqueezing transform", *Anal. Appl.*, vol. 19, no. 1, pp. 71-105, 2021.
- [39] G. Yu, M. Yu, C. Xu, "Synchroextracting transform", *IEEE Trans. Ind. Electron.*, vol. 64, no. 10, pp. 8042-8054, 2017.
- [40] C. Li, M. Liang, "A generalized synchrosqueezing transform for enhancing signal time-frequency representation", *Signal Process.*, vol. 92, pp. 2264-2274, 2012.
- [41] S. Wang, X. Chen, G. Cai, B. Chen, X. Li, Z. He, "Matching demodulation transform and synchrosqueezing in time-frequency analysis", *IEEE Trans. Signal Process.*, vol. 62, no. 1, pp. 69-84, 2014.
- [42] T. Oberlin, S. Meignen, V. Perrier, "Second-order synchrosqueezing transform or invertible reassignment? Towards ideal time-frequency representations", *IEEE Trans. Signal Process.*, vol. 63, no. 5, pp. 1335-1344, 2015.
- [43] D.H. Pham, S. Meignen, "High-order synchrosqueezing transform for multicomponent signals analysis-with an application to gravitational-wave signal", *IEEE Trans. Signal Process.*, vol. 65, no. 12, pp. 3168-3178, 2017.
- [44] G. Yu, Z. Wang, P. Zhao, "Multi-synchrosqueezing transform", *IEEE Trans. Ind. Electron.*, vol. 66, no. 7, pp. 5441-5455, 2019.
- [45] W. Zhang, T. Wu, B. Zhang, H. Luo, "Multiple squeezing based on velocity synchronous chirplet transform with application for bearing fault diagnosis", *Mech. Syst. Signal Process.*, vol. 188, 2023, no. 110006.
- [46] D. He, H. Cao, S. Wang, X. Chen, "Time-reassigned synchrosqueezing transform: The algorithm and its applications in mechanical signal processing", *Mech. Syst. Signal Process.*, vol. 117, pp. 255-279, 2019.
- [47] H. Dong, G. Yu, Y. Li, "Theoretical analysis and comparison of transient-extracting transform and time-reassigned synchrosqueezing transform", *Mech. Syst. Signal Process.*, vol. 178, 2022, no. 109190.
- [48] X. Zhu, Z. Zhang, Z. Li, J. Gao, X. Huang, G. Wen, "Multiple squeezes from adaptive chirplet transform", *Signal Process.*, vol. 163, pp. 26-40, 2019.
- [49] X. Zhu, Z. Zhang, J. Gao, B. Li, Z. Li, X. Huang, G. Wen, "Synchroextracting chirplet transform for accurate IF estimate and perfect signal reconstruction", *Dig. Signal Process.*, vol. 93, pp. 172-186, 2019.
- [50] X. Zhu, B. Li, K. Yang, Z. Zhang, W. Li, "Parameter analysis of chirplet transform and high-resolution time-frequency representation via chirplets combination", *Signal Process.*, vol. 205, 2023, no. 108824.
- [51] Z. Meng, M. Lv, Z. Liu, F. Fan, "General synchroextracting chirplet transform: Application to the rotor rub-impact fault diagnosis", *Measurement*, vol. 169, 2021, no. 108523.
- [52] Y. Jiang, W. Chen, M. Li, T. Zhang, Y. You, "Synchroextracting chirplet transform-based epileptic seizures detection using EEG", *Biomed. Signal Process. Control*, vol. 68, 2021, no. 102699.
- [53] Z. Li, J. Gao, Z. Wang, "A time-synchroextracting transform for the time-frequency analysis of seismic data", *IEEE Geo. Remo. Sens. Lett.*, vol. 17, no. 5, pp. 864-868, 2020.
- [54] V.V. Moca, H. Bârzan, A. Nagy-Dăbâcan, R. CMureşan, "Time-frequency super-resolution with superlets", *Nat. Commun.*, vol. 12, 2021, no. 337.
- [55] L. Li, C.K. Chui, Q.T. Jiang, "Direct signals separation via extraction of local frequencies with adaptive time-varying parameter", *IEEE Trans. Signal Process.*, vol. 70, pp. 2321-2333, 2022.
- [56] P.E. Gill, W. Murray, M.H. Wright, *Practical optimization*, Academic Press, 1982.
- [57] C.K. Chui, H.N. Mhaskar, "Signal decomposition and analysis via extraction of frequencies", *Appl. Comput. Harmon. Anal.*, vol. 40, no. 1, pp. 97-136, 2016.
- [58] N. Hurley, S. Rickard, "Comparing measures of sparsity", *IEEE Trans. Inform. Theory*, vol. 55, no. 10, pp. 4723-4741, 2009.
- [59] B. Boashash, S. Ouelha, "An improved design of high-resolution quadratic time-frequency distributions for the analysis of nonstationary multicomponent signals using directional compact kernels", *IEEE Trans. Signal Process.*, vol. 65, no. 10, pp. 2701-2713, 2017.
- [60] M. Mohammadi, N. Ali Khan, A.A. Pouyan, "Automatic seizure detection using a highly adaptive directional time-frequency distribution", *Multidim. Syst. Sig. Process.*, vol. 29, pp. 1661-1678, 2018.
- [61] B.P. Abbott, R. Abbott, T. D. Abbott, et al, "Observation of gravitational waves from a binary black hole merger", *Phys. Rev. Lett.*, vol. 116, pp. 1-16, 2016.